Towards an improved soil moisture retrieval for organic-rich soils from SMOS passive microwave L-band observations

Simone Bircher*[1], Philippe Richaume[1], Ali Mahmoodi[1], Arnaud Mialon[1], Roberto Fernandez-Moran[2,3], Jean-Pierre Wigneron[2], François Demontoux[4], François Jonard[5,6], Lutz Weihermüller[5], Mie Andreasen[7], Kimmo Rautiainen[8], Jaakko Ikonen[8], Virginie Moreaux[9], Yongwon Kim[10], Bang-Yong Lee[11], Rikie Suzuki[12], Hiroki Ikawa[13], Walter Oechel[14], Luca Belelli Marchesini[15,16], Han Dolman[15], Zhongbo Su[17], Yijian Zeng[17], Rogier van der Velde[17], Mike Schwank[18], Matthias Drusch[19], Yann H. Kerr[1]

[1]CESBIO, Université de Toulouse, CNES/CNRS/IRD/UPS , Toulouse, France ; [2]INRA, UR1391 ISPA, Villenave d'Ornon, Centre INRA Bordeaux Aquitaine, France ; [3]University of Valencia. Faculty of Physics. Dept. of Earth Physics & Thermodynamics. Climatology from Satellites Group, Valencia, Spain; [4]Laboratoire de l'Intégration du Matériau au Système, Bordeaux University, Talence, France; [5]Agrosphere (IBG-3), Institute of Bio- and Geosciences, Forschungszentrum Jülich GmbH, Germany; [6]Earth and Life Institute, Unviersité catholique de Louvain, Louvain-la-Neuve, Belgium; [7]Department of Geosciences and Natural Resource Management, University of Copenhagen, Denmark; [8]Finnish Meteorological Institute, Helsinki, Finland; [9]UMR1137 d'Ecologie et Ecophysiologie Forestières, Institut National de la Recherche Agronomique, Champenoux, France; [10]International Arctic Research Center, University of Alaska Fairbanks, AK, USA; [11]Arctic Research Center, Korea Polar Research Institute, Incheon, Korea;[12]Dept. of Environ. Geochemical Cycle Research, Japan Agency for Marine-Earth Science and Technology, Yokohama, Japan; [13]Agro-Meteorology Division, National Institute for Agro-Environmental Sciences, Tsukuba, Ibaraki, Japan; [14]Global Change Research Group, San Diego State University, San Diego, CA, USA; [15]Department of Earth Sciences, VU University Amsterdam, Amsterdam, The Netherlands; [16]School of Natural Sciences, Far Eastern Federal University, Ajax st. Russky Island, Vladivostok, Russia; [17]University of Twente, Faculty of Geo-Information Science and Earth Observation, AE Enschede, The Netherlands; [18]Swiss Federal Institute for Forest, Snow and Landscape Research, Birmensdorf, Switzerland; [19]European Space Agency, ESTEC, Noordwijk, The Netherlands;
contact: simone.bircher@cesbio.cnes.fr

Introduction

From the passive L-band microwave radiometer onboard the Soil Moisture and Ocean Salinity (SMOS) satellite global surface soil moisture and vegetation optical depths τ data are retrieved at a spatial resolution of ~40 km every ~3 days. Thus far, the dielectric model applied in the retrieval algorithm to relate soil moisture θ to soil relative permittivity ε (relative and imaginary parts ε''/ε', respectively) only accounts for mineral soils. However, especially in the higher Northern latitudes pronounced organic soil surface layers are present. Soil moisture monitoring over these regions is crucial since they are highly sensitive to climate change. Due to differing structural characteristics and thus varying bound water fractions, ε of organic material is lower than that of the most mineral soils. Therefore, an empirical dielectric model for organic substrates was derived based on θ -ε L-band measurements of various samples using a resonant cavity (Bircher et al. 2016). Here, we firstly present SMOS soil moisture retrievals using a simplified processing scheme and either the default dielectric model for mineral soils (Mironov et al. 2013) or the newly developed "organic" model (Figure 1). These datasets are compared with the operational SMOS product as well as in situ soil moisture data from organic surface layers over selected validation sites (Figure 2). Secondly, we present an approach to create a global map of the presence of organic surface layers based on Soil Organic Carbon (SOC) as well as soil, climate and forest class information, in order to decide where a soil moisture retrieval using the "organic" dielectric model should be triggered.

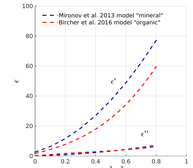

Figure 2: Mironov "mineral" dielectric model used in the SMOS soil moisture retrieval versus simple empirical "organic" dielectric model. Mironov model settings: soil bulk density: 1.270 g/cm³, soil particle density: 2.664 g/cm³, pure water temperature: 20 °C, clay/sand %: 1.3/88

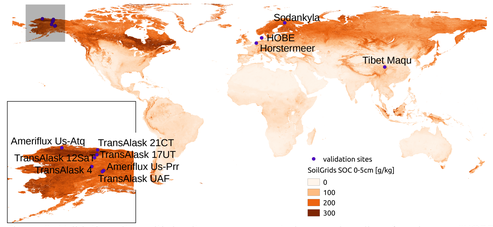

Figure 2: Validation sites with in situ measurements in organic soil surface layers. "HOBE" is used as reference site with mainly mineral soils. Base map: SoilGrids Soil Organic Carbon (ORCDRC) product, 0-5 cm depth composite (Hengl et al. 2017)

Soil moisture product comparison

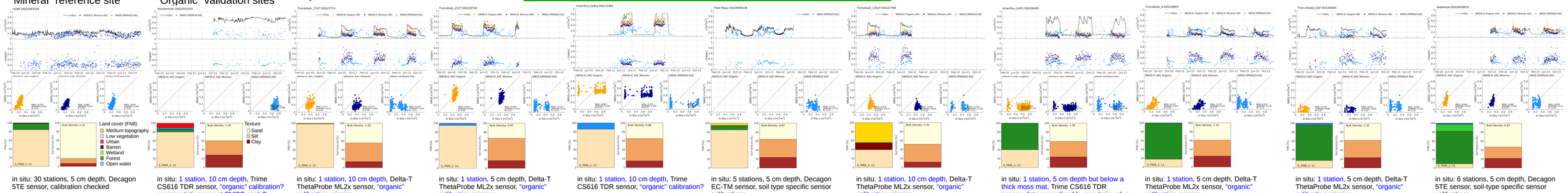

in situ: 30 stations, 5 cm depth, Decagon 5TE sensor, calibration checked

in situ: 1 station, 10 cm depth, Trime CS616 TDR sensor, "organic" calibration? representativeness at SMOS scale?
SMOS-IC: No retrieval due to urban and water fractions > 10%

in situ: 1 station, 10 cm depth, Delta-T ThetaProbe ML2x sensor, "organic" calibration missing

in situ: 1 station, 5 cm depth, Delta-T ThetaProbe ML2x sensor, "organic" calibration missing

in situ: 1 station, 10 cm depth, Trime CS616 TDR sensor, "organic" calibration?

in situ: 5 stations, 5 cm depth, Decagon EC-TM sensor, soil type specific sensor calibrations
SMOS: contaminated by man-made Radio-Frequency Interference (RFI)

in situ: 1 station, 10 cm depth, Delta-T ThetaProbe ML2x sensor, "organic" calibration missing

in situ: 1 station, 5 cm depth but below a thick moss mat, Trime CS616 TDR sensor, data normalized by max/min value for each year

in situ: 1 station, 5 cm depth, Delta-T ThetaProbe ML2x sensor, "organic" calibration missing

in situ: 1 station, 5 cm depth, Delta-T ThetaProbe ML2x sensor, "organic" calibration missing

in situ: 6 stations, 5 cm depth, Decagon 5TE sensor, soil-type specific sensor calibrations

Figure 3: Temporal series of in situ soil moisture θ, SMOS retrieved soil moisture using a simplified processing scheme (SMOS-IC) and either the Mironov dielectric model for mineral soils or the "organic" model, as well as data from the operational SMOS level 2 soil moisture product V620 (SMOS OPER620), ascending (ASC) overpasses only, for the HOBE reference site with mainly mineral soils and selected validation sites (Figure 2) with in situ sensors in organic soil surface layers (first row), respective temporal series of SMOS retrieved optical depths τ (second row), corresponding soil moisture scatter plots (third row), and land cover (FN0) fractions as well as soil properties (texture and bulk density) assumed in the operational SMOS soil moisture processor (Kerr et al. 2014) at the respective sites (fourth row). S_TREE_1 indicates whether a low vegetation (12) or forest (11) retrieval is triggered in the operational SMOS processor. SMOS-IC treats each satellite pixel as homogeneous surface, but vegetation and roughness parameter settings are based on a weighted average of prevailing land cover classes. The Discrete Global Grid (DGG) id of the SMOS level 2 pixels corresponding to the selected sites are given. The closest SMOS-IC grid point is chosen (EASE-Grid 2.0). The SMOS OPER620 product is filtered where the scaled Chi2 probability<0.1, SM_DQX=NaN, and flag NOPROD=1. The SMOS-IC product is filtered where the quality flag≠0. Some additional information is provided for each site. Factors hampering the comparison of in situ and SMOS data are highlighted in blue.

Global organic surface layer map

SoilGrids TAXNWRB (Hengl et al. 2017: World Reference Base Soil Classes, based on second edition, IUSS Working Group WRB 2006)

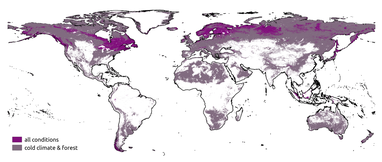

Figure 4: SoilGrids TXNWRB soil classes estimated to exhibit organic soil surface layers under all conditions, as well as in the cold climate zones and/or under coniferous/mixed forest, respectively.

Soil Classes	Organic Surface Layer: all conditions	Organic Surface Layer: cold climate zones and/or coniferous/mixed forest
Albeluvisols		x
Andosols		x
Arenosols		x
Cambisols		x
Cryosols		x
Gleysols		x
Histosols	x	
Luvisols		x
Phaeozems		x
Podzols	x	
Umbrisols		x

Köppen-Geiger Climate Classes 1986-2010 (Climatic Research Unit of the University of East Anglia & Global Precipitation Climatology Centre, German Weather Service, http://koeppen-geiger.vu-wien.ac.at/present.htm)

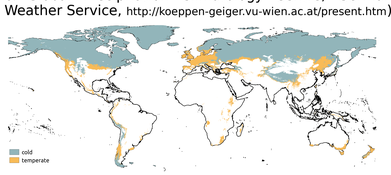

Figure 5: Köppen-Geiger climate classes estimated to belong to the cold and temperate climate zones, respectively.

IGBP Land Cover (Broxton et al. 2014: based on MODIS Land Cover Product MCD12Q1 & Int. Geosphere-Biosphere Programme class labels)

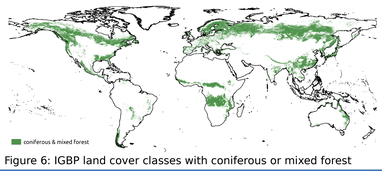

Figure 6: IGBP land cover classes with coniferous or mixed forest

Class ID	Description	Climate Zone: Cold	Climate Zone: Temperate
Cfb	Temperate oceanic climate		x
Cfc	Subpolar oceanic climate	x	
Csb	Warm-summer mediterranean climate		x
Csc	Cool-summer mediterranean climate		x
Cwb	Subtropical highland climate or temperate oceanic climate with dry winters		x
Cwc	Cold subtropical highland climate or subpolar oceanic climate with dry winters	x	
Dfa	Hot-summer humid continental climate		x
Dfb	Warm-summer humid continental climate	x	
Dfc	Subarctic climate	x	
Dfd	Extremely cold subarctic climate	x	
Dsa	Hot, dry-summer continental climate		x
Dsb	Warm, dry-summer continental climate		x
Dsc	Dry-summer subarctic climate	x	
Dsd	Extremely cold, dry-summer subarctic climate	x	
Dwa	Monsoon-influenced hot-summer humid continental climate		x
Dwb	Monsoon-influenced warm-summer humid continental climate		x
Dwc	Monsoon-influenced subarctic climate	x	
Dwd	Monsoon-influenced extremely cold subartic climate	x	
EF	Ice cap Climate	x	
ET	Mild tundra climate	x	

Considered forest classes	Class code
Evergreen Needle Leaf Forest	1
Deciduous Needle Leaf Forest	3
Mixed Forest	5
Woody Savanna (including Boreal Forest)	8

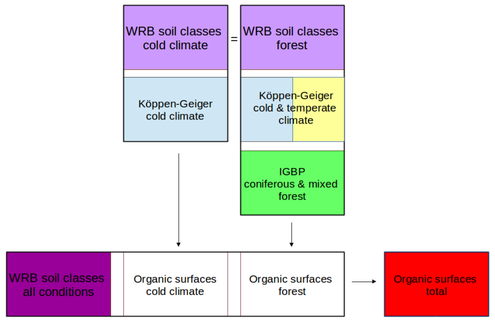

Figure 7: Merging of the soil, climate, and forest class information (Figures 4-6) in order to create a global map of the presence of organic soil surface layers. The three categorical input maps are previously resampled to 0.01 x 0.01 degree (~1 x 1 km) pixel size (class type appearing most often is selected) and adjusted to the same extent (180W – 180E/90N – 62S). With respect to coniferous and mixed forest, organic soil surface layers are expected to appear in the cold and temperate climate zones, while a too fast turnover for accumulation of organic layers is assumed under tropical forest.

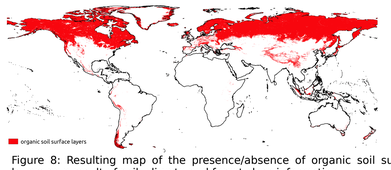

Figure 8: Resulting map of the presence/absence of organic soil surface layers as a result of soil, climate and forest class information.

Highest spatial correlation R between the organic soil surface layer map (Figure 8) and the SoilGrids 0-5 cm SOC product (ORCDRC, Figure 2) is achieved for an SOC threshold of 102 g/kg (R=0.93)

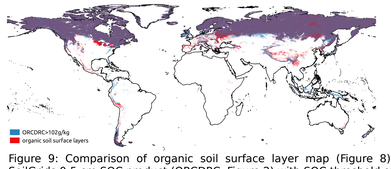

Figure 9: Comparison of organic soil surface layer map (Figure 8) and SoilGrids 0-5 cm SOC product (ORCDRC, Figure 2) with SOC threshold of 102 g/kg. Purple zones show agreement between the two maps. The ORCDRC map is also previously resampled to 0.01 x 0.01 degree pixel size (average of all contributing pixels) and extended to 180W – 180E/90N – 62S.

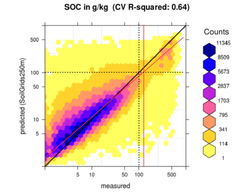

Figure 10: Performance of the SoilGrid SOC (ORCDRC) product. Figure adapted from Hengl et al. 2017: Correlation density plot resulting from a model re-fitted 10 times using 90% of the available soil profile observations compared with the remaining 10%.

At an SOC threshold of 102g/kg (10%) underestimation of the SoilGrids SOC product lies in the order of ~25 g/kg (Figure 10), resulting in a corrected threshold of ~127 g/kg (12.7%). Based on definitions by the World Soil Reference Base and the Soil Science Society of America, the SOC treshold between organic and mineral soil material should lie between 11.6 and 20.3 % (116-203 g/kg SOC) → The corrected SoilGrids ORCDRC SOC treshold lies within the expected range.

Conclusions

Soil moisture product comparison: Over the "organic"validation sites, there is a tendency towards SMOS dry bias compared to in situ measurements, with the SMOS-IC product showing somewhat better temporal trends than the SMOS OPER620 product. Where the open water fraction starts becoming important the SMOS-IC soil moisture is increased as this algorithm does not (yet) correct for open water. The use of the "organic" dielectric model raises soil moisture levels, though, at the very low SMOS soil moisture values, the difference compared to the processing with the Mironov "mineral" model stays minor, while it would be more significant in the soil moisture range of the in situ observations (see Figure 1). The in situ observations are often not ideal themselves with mainly only 1 sensor per large satellite footprint and no specific sensor calibration applied for the organic substrate. Organic soil surface layer map: As a starting point it is suggested to use the SoilGrids Soil Organic Carbon (ORCDRC) 0-5cm depth map with a threshold of 102 g/kg in the SMOS soil moisture processor. The SoilGrids ORCDRC product is derived from a wealth of covariates and a sophisticated approach and will most likely further improve in the future, whereas the here derived organic soil surface layer map is based on a very simple approach. But (due to the high spatial correlation between the two maps) the latter will be useful to evaluate a potential SoilGrids ORCDRC threshold change once the latter will be updated. In a next step the SoilGrids ORCDRC map will be implemented in the SMOS soil moisture processor to test a switch between the "mineral" and "organic" dielectric models.

References: Bircher et al. 2016, Remote Sensing, 8(12), 1024. Broxton et al. 2014, Journal of Applied Meteorology and Climatology, 53, 1593-1605. Hengl et al. 2017, PLOS ONE, 12(2), e0169748. IUSS Working Group WRB 2006, World Reference Base for Soil Resources, Report No. 103, FAO, Rome, Italy. Kerr et al. 2014, SMOS level 2 processor Soil Moisture Algorithm Theoretical Basis Document V4.a, SM-ESL (CBSA), Toulouse, France, 142p. Mironov et al. 2013, IEEE Geoscience and Remote Sensing Letters, 10, 419-423. Acknowledgements: ESA STSE Changing Earth Science Network & ESL; CNES TOSCA, France